

Controls on Sea-Air CO₂ Flux in EBUS

Riley X. Brady

July 3, 2017

Abstract

I am working to understand what controls historical variability in Sea-Air CO₂ Flux in Eastern Boundary Upwelling Systems. I use FG_CO2 output from the CESM Large Ensemble and correlate/regress it against various climate indices derived from model output (using Adam Phillip's CESM-LE CVDP output). In total, we have 34 ensemble members to work with, and treat them as independent time series.

1 Model Evaluation

Figure 1 compares 30-year annual climatologies of sea-air CO₂ flux (FGCO₂) across the four upwelling systems (spanning 1982-2011). The top row is derived from the 30-year monthly resolution neural network, described in Landschützer et al. [2013]. The bottom row is the ensemble mean of 34 members of the CESM Large Ensemble spanning the same time period.

The Pacific Ocean systems seem to be best represented by the CESM-LE. For the CalCS, we find a gradient between equatorward outgassing and poleward uptake. Since we are truly focused on the northern HumCS—an area of warm, tropical SSTs and strong upwelling—we find persistent outgassing. For the CanCS, the observational product represents fairly weak CO₂ flux all together, and is characterized by a meridional gradient between equatorward outgassing and poleward uptake. On the other hand, the model product simulates more intense CO₂ uptake overall, and is more characterized by a zonal gradient between coastal outgassing and offshore uptake. Lastly, the BenCS is quite similar to the CalCS observationally, with uptake toward the poles and outgassing toward the equator. The model does simulate this, but has a much steeper gradient between the two regions, and more intense outgassing overall.

There are a few caveats in this comparison. Firstly, the neural network product uses a number of independent predictors (*e.g.*, SST, CHL, MLD, and SSS) to estimate the monthly resolution $p\text{CO}_2$; it isn't a truly observational product that can be treated as truth. Secondly, the neural network product omits coastal regions, so perhaps we might see stronger coastal signals in the CanCS and BenCS to match the model (note that Laruelle et al. [2017] will release a coastal interpolation product). Lastly, the comparison itself is not perfect. We can treat the neural network product as one ‘realization’ of the climate system, which contains the influence of multi-decadal climate variability and external forcing. On the other hand, the model climatology averages out most of the internal variability, leaving us with a picture of the externally forced climatology. Perhaps a better comparison would be with one realization of the CESM-LE, but how does one choose the appropriate realization for comparison?

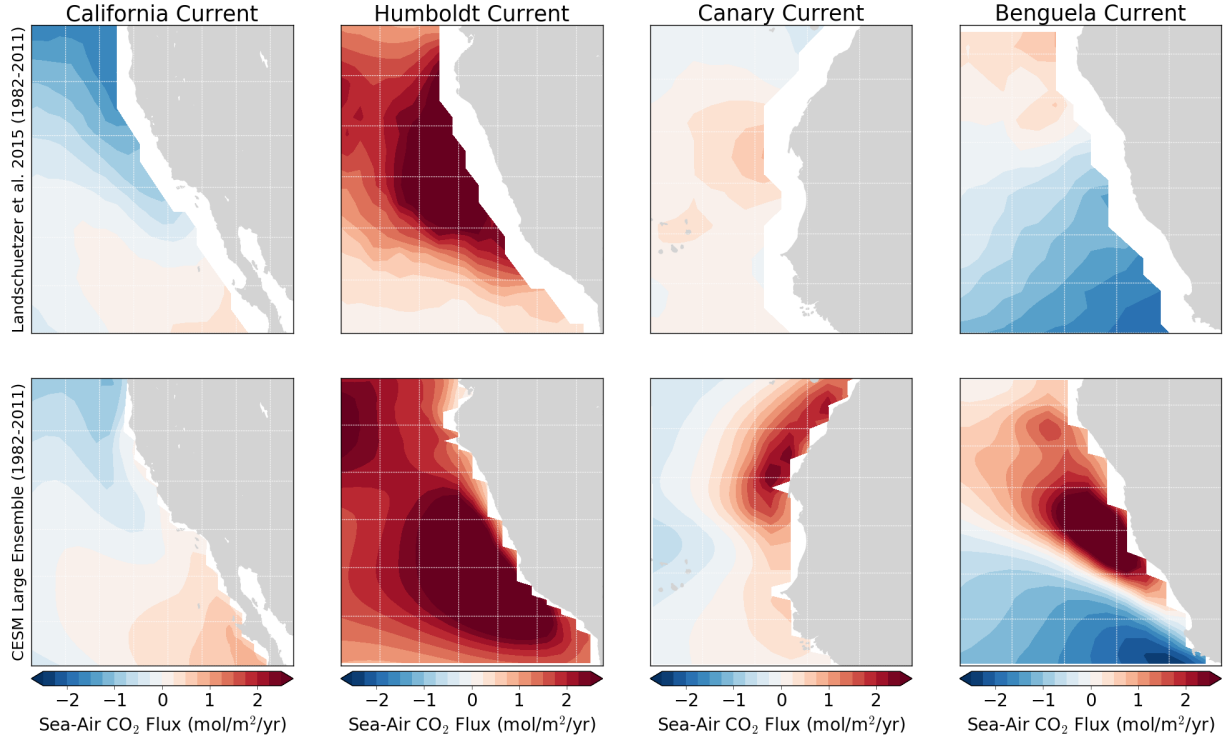


Figure 1: Annual averages of Sea-Air CO₂ flux over 1982-2011 for the four major eastern boundary upwelling systems. The top row is observational data from Landschützer et al. [2013], while the bottom row is the ensemble mean from the CESM Large Ensemble. Red colors represent outgassing of CO₂, while blue colors represent uptake.

2 Study Sites

For simplicity, I am using the latitudinal bounds set up by Chavez and Messié [2009], which dictates the ten degrees of most active upwelling via satellite wind stress climatology. I then constrain the offshore region to within 800km (via cell width output from the model).

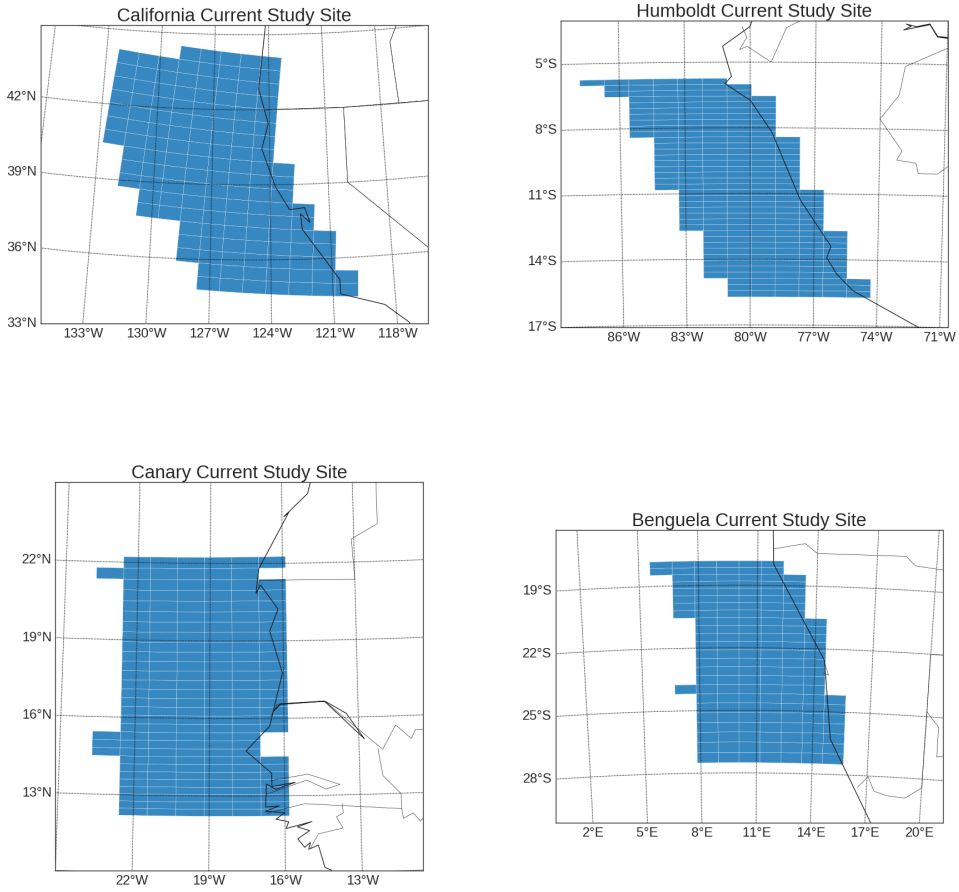


Figure 2: Nearshore regions for each EBUS over which area-weighted FGCO₂ is computed. The latitude is constrained by the 10 degree bounds of most active upwelling (per Chavez and Messié [2009]). The longitude is constrained to 800km offshore to standardize region sizes across different latitudes.

3 General Methodology

We use 34 CESM-LENS members, which can be treated as entirely independent time series, spanning 1920-2100 at monthly resolution. We focus, however, on the 1920-2015 period, since we are trying to understand the historical controls on FGCO₂ variability (and as Adam Phillip's CVDP package covers this same period). The area-weighted mean (using TAREA) of FGCO₂ is computed for each EBUS, generating a 34x1152 time series matrix.

First, we subtract the ensemble mean time series from each individual simulation. This de-trends and de-seasonalizes the data, leaving us with 34 independent anomaly time series, which we can think of as the *natural* flux of CO₂ into and out of the coastal ocean (e.g.

Figure 3 and Figure 4). We then load in climate index time series (Nino3.4, PDO, AMO, NAO, SAM) for the same ensemble members, and remove the linear trend from each to similarly produce anomaly time series.

We apply a 12-month (annual) rolling mean to all FGCO₂ anomaly time series, as we find the raw time series to be much too noisy for meaningful correlations. See Figure 5, which demonstrated raw (color) time series for simulation 001 for each EBUS and the smoothed time series overlaid in black. This is defensible, as an FFT of these raw time series shows roughly red noise.

Lastly, we regress the smoothed FGCO₂ anomalies onto the four main predictors: Nino3.4, PDO, AMO, and SAM.

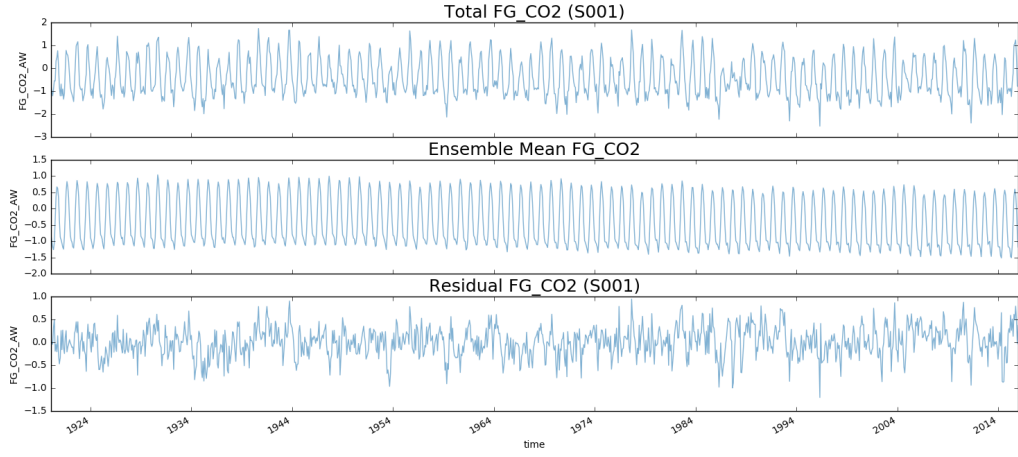


Figure 3: Decomposed time series for simulation 001 of CalCS FGCO2. The first panel is the total simulated FGCO2 over the historical period. The second panel is the ensemble mean, displaying the trended and seasonalized component. The last plot is the residual flux after subtracting the second plot. This is what we base our correlations on and consider the natural flux.

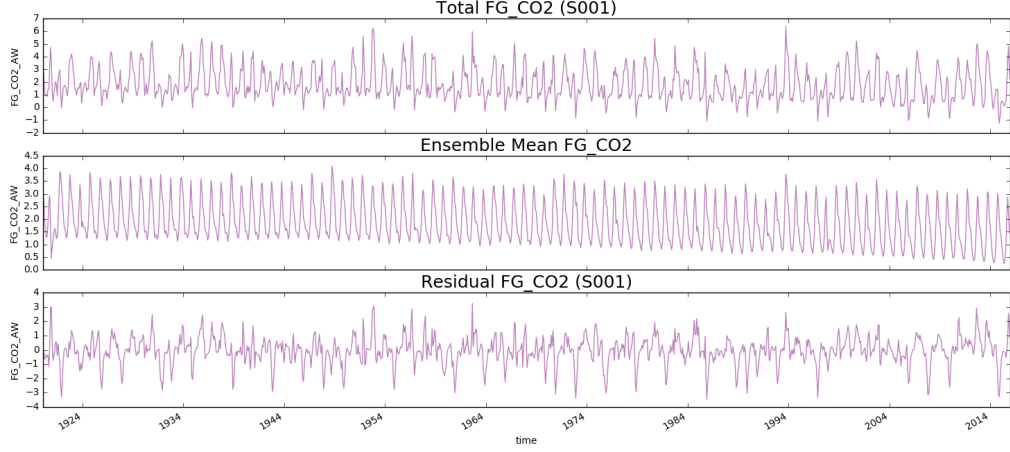


Figure 4: Decomposed time series for simulation 001 of BenCS FGCO2. The first panel is the total simulated FGCO2 over the historical period. The second panel is the ensemble mean, displaying the trended and seasonalized component. The last plot is the residual flux after subtracting the second plot. This is what we base our correlations on and consider the natural flux.

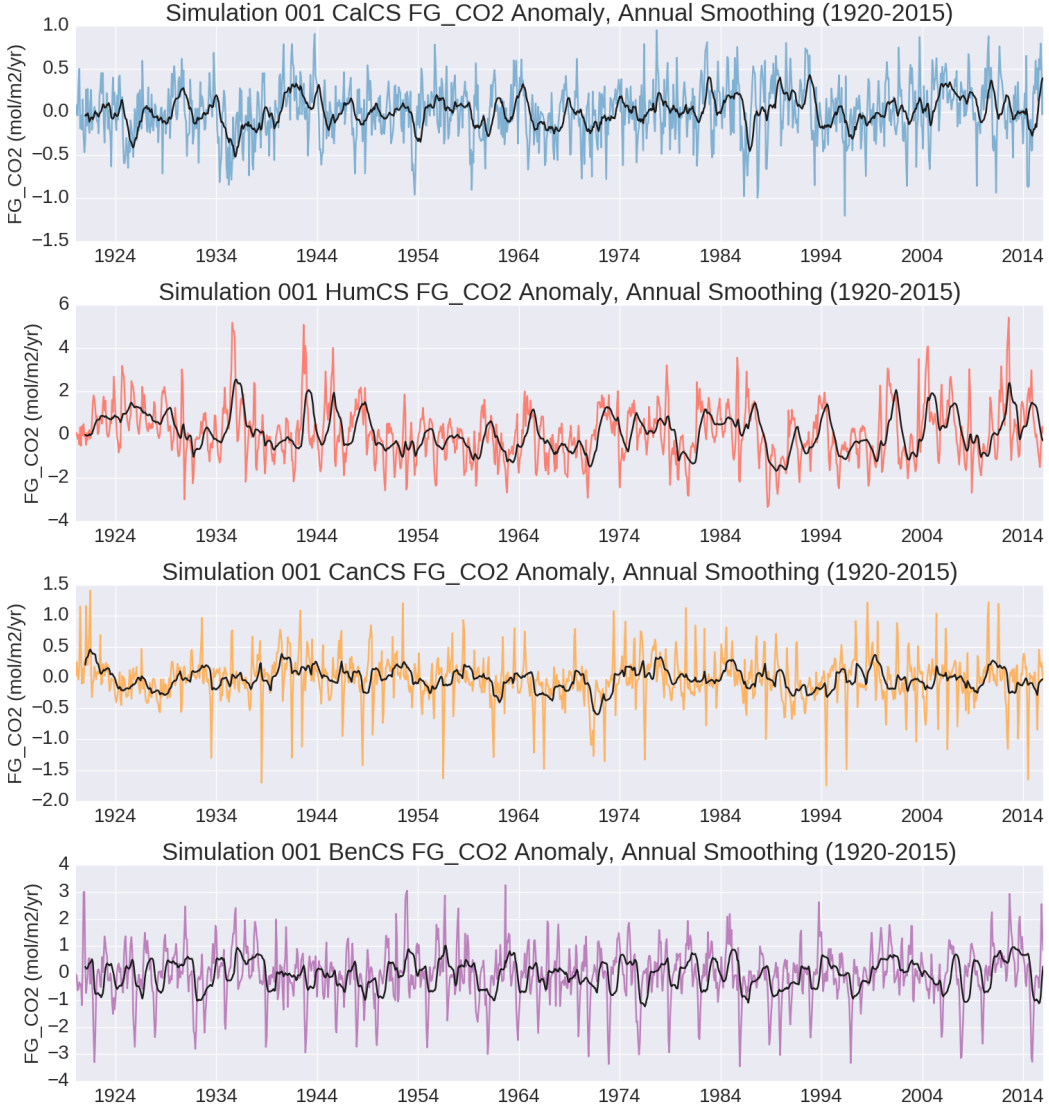


Figure 5: FGCO₂ anomalies for arbitrary simulation 001 in color with their annual smoothing counterpart overlaid in black.

4 Climate Correlations

I have split the analysis into the two major ocean basins that house our four EBUS. This is because (1) it eases the viewing and interpretation of statistical tests, and (2) we might glean some similarities and differences between the two basins.

4.1 Pacific Sector

Figure 6 displays the results of using four climate indices (Nino3.4, PDO, AMO, and SAM) as predictors for CalCS and HumCS natural CO₂ fluxes over the 1920-2015 period. We find

that ENSO and PDO have the largest influence on natural CO₂ flux variability, and have inverse impacts on the two systems.

During an El Niño event, more CO₂ fluxes out of the CalCS, while more CO₂ is taken up by the HumCS. Perhaps this illuminates the dependency of CalCS FGCO₂ on SST variability, which would alter the solubility of pCO₂; during a warm event, low pCO₂ solubility would force carbon out of the CalCS. On the other hand, SSTs might be more stable in the more tropical HumCS, so FGCO₂ variability could be more dependent on DIC delivery from depth. During El Niño events, upwelling of high-DIC water would be suppressed, leading to an influx of carbon. These ideas can be tested by using Takahashi formulae to separate temperature-dependent pCO₂ effects from non-temperature-dependent effects. These arguments might also hold for the PDO, since it has a large impact on Pacific Ocean SST patterns. Raw values for the regression slope, r-value, and r² can be found in Table 1 (Nino3.4) and Table 2 (PDO).

An interesting result is that AMO has a small, but discernible correlation with CalCS CO₂ flux, but hovers around an r-value of zero for the HumCS. Perhaps atmospheric teleconnections between the North Atlantic and North Pacific play a role here.

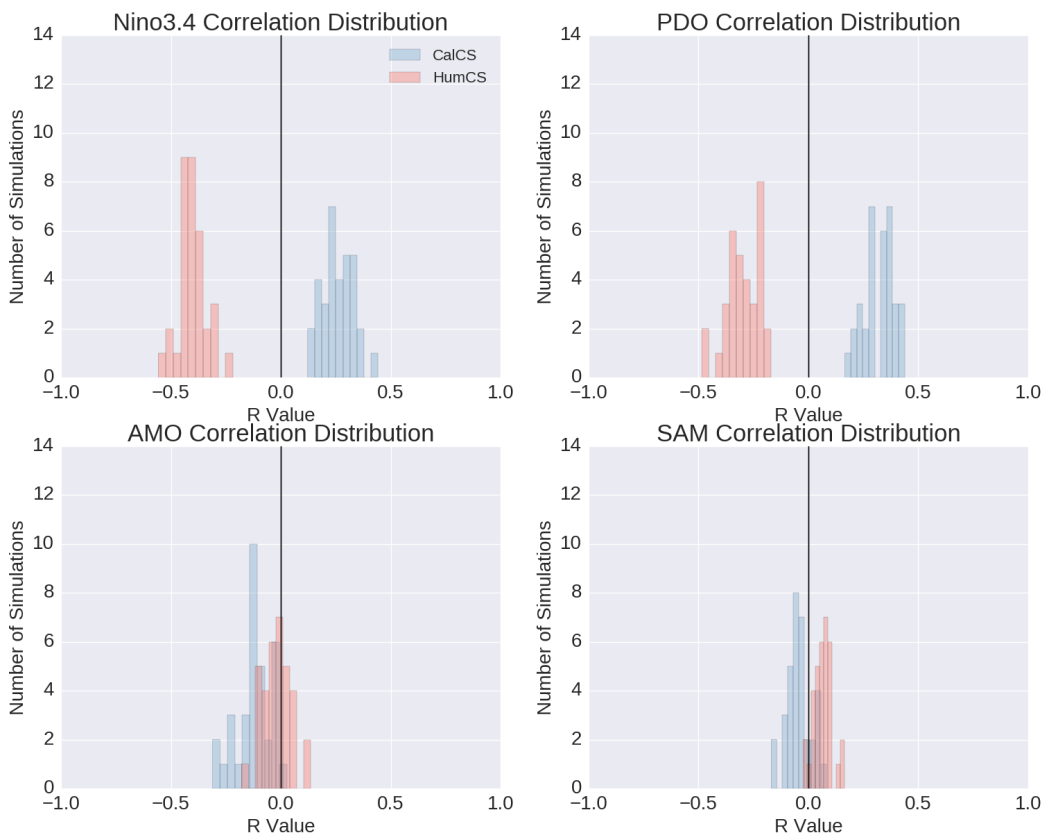


Figure 6: R values for annually smoothed FGCO₂ anomalies in the CalCS and HumCS compared to four major climate indices. Correlations with $p > 0.05$ were not included.

Table 1: Results for regressing FGCO₂ anomalies onto Niño3.4 time series for the two Pacific upwelling systems. Results with $p > 0.05$ are excluded.

Simulation	CalCS			HumCS		
	Slope ^a	R	R ²	Slope ^a	R	R ²
001	0.04	0.30	0.09	-0.20	-0.29	0.08
002	0.06	0.33	0.11	-0.31	-0.35	0.12
009	0.03	0.18	0.03	-0.24	-0.31	0.10
010	0.04	0.22	0.05	-0.33	-0.44	0.19
011	-	-	-	-0.28	-0.39	0.15
012	0.05	0.28	0.08	-0.31	-0.43	0.19
013	0.06	0.33	0.11	-0.33	-0.42	0.17
014	0.05	0.35	0.12	-0.30	-0.44	0.19
015	0.05	0.29	0.08	-0.34	-0.44	0.20
016	0.04	0.22	0.05	-0.32	-0.38	0.14
017	0.04	0.27	0.07	-0.26	-0.45	0.20
018	0.05	0.29	0.08	-0.33	-0.40	0.16
019	0.04	0.21	0.04	-0.35	-0.43	0.19
020	0.05	0.30	0.09	-0.22	-0.36	0.13
021	0.03	0.18	0.03	-0.28	-0.36	0.13
022	0.04	0.24	0.06	-0.37	-0.46	0.22
023	0.03	0.22	0.05	-0.31	-0.37	0.14
024	0.06	0.33	0.11	-0.33	-0.44	0.19
025	0.05	0.34	0.12	-0.29	-0.40	0.16
026	0.04	0.25	0.06	-0.32	-0.39	0.15
027	0.04	0.28	0.08	-0.22	-0.30	0.09
028	0.03	0.17	0.03	-0.26	-0.38	0.15
029	0.05	0.33	0.11	-0.39	-0.46	0.21
030	0.03	0.19	0.04	-0.30	-0.42	0.17
031	0.04	0.24	0.06	-0.34	-0.42	0.18
032	0.04	0.20	0.04	-0.39	-0.51	0.26
033	0.02	0.14	0.02	-0.14	-0.22	0.05
034	0.06	0.31	0.10	-0.25	-0.32	0.10
035	0.03	0.17	0.03	-0.31	-0.42	0.18
101	0.07	0.44	0.20	-0.28	-0.41	0.17
102	0.04	0.26	0.07	-0.24	-0.40	0.16
103	0.04	0.22	0.05	-0.29	-0.40	0.16
104	0.05	0.35	0.12	-0.41	-0.56	0.31
105	0.02	0.12	0.01	-0.45	-0.49	0.24
Mean	0.04	0.26	0.07	-0.30	-0.40	0.17
Std	0.01	0.07	0.04	0.06	0.06	0.05

^a mol/m²/yr/degC

Table 2: Results for regressing FGCO₂ anomalies onto PDO time series for the two Pacific upwelling systems. Results with $p > 0.05$ are excluded.

Simulation	CalCS			HumCS		
	Slope ^a	R	R ²	Slope ^a	R	R ²
001	0.06	0.38	0.14	-0.23	-0.28	0.08
002	0.06	0.35	0.12	-0.20	-0.24	0.06
009	0.06	0.36	0.13	-0.17	-0.22	0.05
010	0.06	0.35	0.12	-0.27	-0.36	0.13
011	0.03	0.17	0.03	-0.29	-0.38	0.14
012	0.07	0.38	0.15	-0.20	-0.25	0.06
013	0.04	0.25	0.06	-0.22	-0.30	0.09
014	0.06	0.34	0.11	-0.25	-0.30	0.09
015	0.05	0.29	0.09	-0.17	-0.23	0.05
016	0.05	0.28	0.08	-0.18	-0.22	0.05
017	0.06	0.37	0.14	-0.23	-0.34	0.11
018	0.05	0.28	0.08	-0.14	-0.17	0.03
019	0.07	0.36	0.13	-0.26	-0.32	0.10
020	0.06	0.37	0.14	-0.26	-0.38	0.15
021	0.04	0.26	0.07	-0.27	-0.35	0.12
022	0.07	0.40	0.16	-0.29	-0.35	0.12
023	0.05	0.37	0.14	-0.16	-0.19	0.04
024	0.08	0.44	0.19	-0.26	-0.34	0.12
025	0.07	0.41	0.17	-0.25	-0.30	0.09
026	0.05	0.33	0.11	-0.17	-0.21	0.04
027	0.03	0.19	0.04	-0.24	-0.29	0.08
028	0.07	0.43	0.19	-0.20	-0.31	0.09
029	0.03	0.22	0.05	-0.26	-0.27	0.07
030	0.05	0.27	0.07	-0.17	-0.23	0.05
031	0.05	0.30	0.09	-0.24	-0.29	0.08
032	0.05	0.29	0.09	-0.35	-0.48	0.23
033	0.05	0.34	0.11	-0.15	-0.21	0.04
034	0.04	0.23	0.05	-0.16	-0.21	0.04
035	0.04	0.23	0.05	-0.17	-0.23	0.05
101	0.05	0.29	0.08	-0.27	-0.35	0.12
102	0.07	0.39	0.15	-0.28	-0.39	0.15
103	0.06	0.34	0.11	-0.25	-0.35	0.12
104	0.06	0.39	0.15	-0.42	-0.48	0.23
105	0.05	0.30	0.09	-0.24	-0.26	0.07
Mean	0.05	0.32	0.11	-0.23	-0.30	0.09
Std	0.01	0.07	0.04	0.06	0.08	0.05

^a mol/m²/yr/degC

4.2 Atlantic Sector

Figure 7 displays distributions of correlation tests between FGCO₂ anomalies in the two Atlantic Ocean EBUS (Canary and Benguela) and the same four climate indices. At first glance, the results are much weaker than that of the Pacific systems. I find it surprising that the SAM has virtually no impact on the BenCS, when it is the only EBUS that interfaces directly with the Southern Ocean.

Interestingly, CanCS gas flux has a reasonable relationship with ENSO and the PDO. As much as 15% of FGCO₂ variability in the CanCS can be explained by ENSO in some simulations (Table 3). We find a similar situation with regards to the PDO (Table 4). There is a slight relationship between FGCO₂ anomalies in the CanCS and the AMO, but it isn't even as strong as the correlation with ENSO and PDO. Overall, the BenCS is not well-explained by any major climate index.

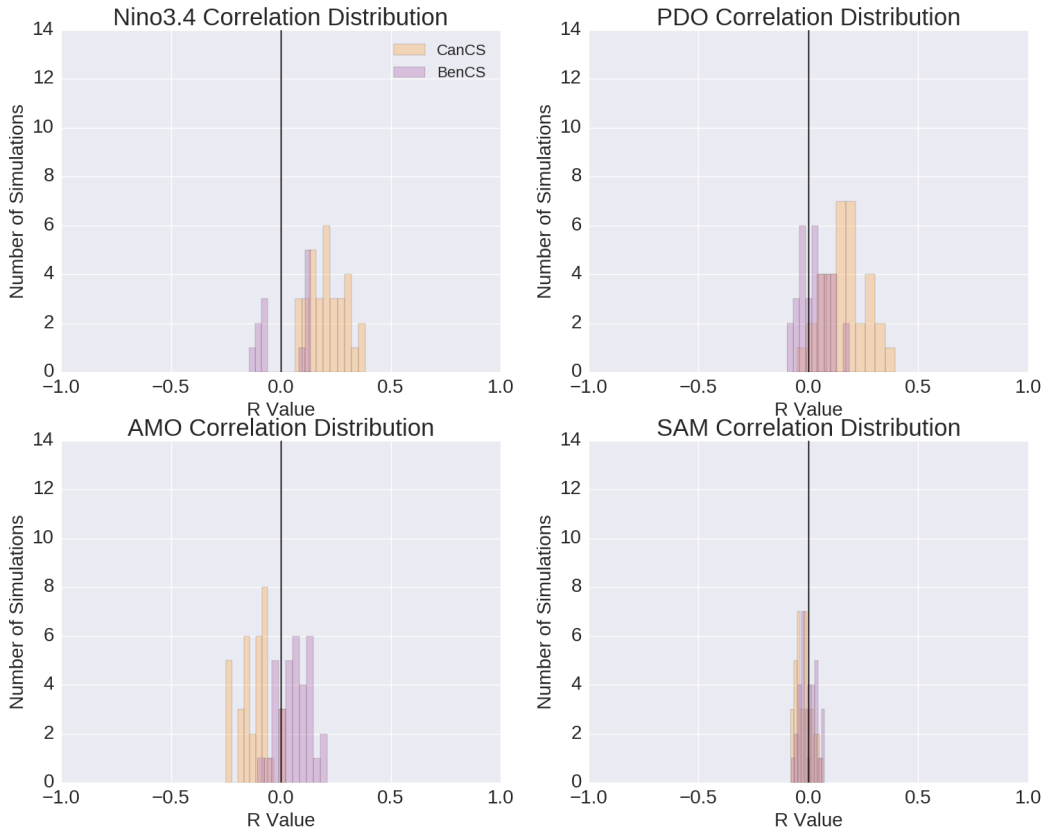


Figure 7: R values for annually smoothed FGCO₂ anomalies in the CalCS and HumCS compared to four major climate indices. Correlations with $p > 0.05$ were not included.

Table 3: Results for regressing FGCO₂ anomalies onto ENSO time series for the two Atlantic upwelling systems. Results with $p > 0.05$ are excluded.

Simulation	CanCS			BenCS		
	Slope ^a	R	R ²	Slope ^a	R	R ²
001	0.04	0.28	0.08	-	-	-
002	0.06	0.31	0.10	-	-	-
009	0.03	0.18	0.03	-	-	-
010	0.05	0.29	0.08	-	-	-
011	0.04	0.25	0.06	0.05	0.13	0.02
012	0.04	0.28	0.08	-0.05	-0.11	0.01
013	0.04	0.22	0.05	-	-	-
014	0.05	0.34	0.12	-	-	-
015	0.03	0.16	0.03	-	-	-
016	0.02	0.10	0.01	-	-	-
017	0.05	0.38	0.15	-	-	-
018	0.03	0.17	0.03	-0.07	-0.14	0.02
019	0.02	0.11	0.01	0.04	0.09	0.01
020	0.05	0.32	0.10	-	-	-
021	0.02	0.12	0.01	-	-	-
022	0.02	0.15	0.02	0.06	0.12	0.01
023	0.04	0.22	0.05	-	-	-
024	0.04	0.25	0.06	0.06	0.13	0.02
025	0.01	0.08	0.01	-	-	-
026	0.05	0.27	0.07	-0.04	-0.09	0.01
027	0.03	0.20	0.04	0.07	0.14	0.02
028	0.01	0.07	0.00	0.06	0.13	0.02
029	0.05	0.31	0.10	-	-	-
031	0.02	0.15	0.02	-	-	-
032	0.03	0.15	0.02	-	-	-
033	0.03	0.21	0.04	-0.03	-0.08	0.01
034	0.03	0.17	0.03	-0.05	-0.11	0.01
035	0.01	0.07	0.00	-0.03	-0.07	0.00
101	0.03	0.22	0.05	-	-	-
102	0.03	0.19	0.04	-	-	-
103	0.07	0.39	0.15	-	-	-
104	0.03	0.23	0.05	-	-	-
105	0.02	0.13	0.02	-	-	-
Mean	0.03	0.21	0.05	0.01	0.01	0.01
Std	0.01	0.09	0.04	0.05	0.11	0.01

^a mol/m²/yr/degC

Table 4: Results for regressing FGCO₂ anomalies onto PDO time series for the two Atlantic upwelling systems. Results with $p > 0.05$ are excluded.

Simulation	CanCS			BenCS		
	Slope ^a	R	R ²	Slope ^a	R	R ²
001	0.05	0.30	0.09	-0.01	-0.02	0.00
002	0.07	0.39	0.15	-0.00	-0.00	0.00
009	0.02	0.11	0.01	-0.03	-0.05	0.00
010	0.05	0.28	0.08	-0.01	-0.01	0.00
011	0.03	0.17	0.03	0.01	0.02	0.00
012	0.02	0.11	0.01	0.02	0.04	0.00
013	0.03	0.21	0.04	0.02	0.03	0.00
014	0.05	0.27	0.07	-0.02	-0.04	0.00
015	0.02	0.11	0.01	0.03	0.07	0.01
016	0.02	0.14	0.02	0.04	0.07	0.01
017	0.04	0.22	0.05	-0.02	-0.05	0.00
018	0.01	0.08	0.01	-0.01	-0.01	0.00
019	0.01	0.06	0.00	0.09	0.19	0.03
020	0.02	0.13	0.02	-0.00	-0.01	0.00
021	0.01	0.06	0.00	0.06	0.13	0.02
022	0.03	0.16	0.03	0.09	0.18	0.03
023	-0.01	-0.05	0.00	-0.01	-0.02	0.00
024	0.02	0.11	0.01	0.04	0.08	0.01
025	0.03	0.17	0.03	-0.04	-0.08	0.01
026	0.02	0.13	0.02	0.02	0.05	0.00
027	0.03	0.19	0.03	0.06	0.10	0.01
028	0.02	0.13	0.02	0.05	0.11	0.01
029	0.06	0.33	0.11	0.06	0.12	0.01
030	0.01	0.05	0.00	0.05	0.10	0.01
031	0.00	0.02	0.00	-0.01	-0.02	0.00
032	0.03	0.20	0.04	-0.03	-0.06	0.00
033	0.03	0.22	0.05	0.01	0.02	0.00
034	0.03	0.14	0.02	-0.05	-0.10	0.01
035	0.02	0.15	0.02	0.02	0.04	0.00
101	0.01	0.04	0.00	0.03	0.05	0.00
102	0.03	0.19	0.03	0.00	0.01	0.00
103	0.05	0.31	0.09	0.06	0.12	0.01
104	0.04	0.27	0.07	0.02	0.03	0.00
105	0.03	0.19	0.04	0.02	0.05	0.00
Mean	0.03	0.16	0.04	0.02	0.03	0.01
Std	0.02	0.09	0.04	0.03	0.07	0.01

^a mol/m²/yr/degC

5 Cross Correlation

Perhaps we are underestimating the strength of relationship between some climate indices and EBU CO₂ flux, as we are not lagging/leading the correlations properly. Due to the physical mechanisms behind ENSO, there might be a sort of lag between a strong El Niño and an anomalous gas flux. Since we are trying to understand controls on CO₂ flux variability, it probably only makes sense to look at situations where the climate index leads the gas flux anomalies.

Figure 8 shows little consistency in enhanced correlations at any lead/lag. I would argue that there is little sense in correlating anything but lag zero in the case of CalCS and Nino3.4. However, turning our attention to the HumCS, we find a strong case to compute a lag correlation for ENSO, rather than a standard lag zero correlation (Figure 9). In 100% of the simulations, the correlation is stronger when leading FGCO₂ anomalies by 4-5 months with the Nino3.4 index.

Table 5 displays the results of a regression analysis between HumCS FGCO₂ anomalies and the Nino3.4 index with a 5-month lead. Without the lead, a 1 degree C El Niño event would explain 17% of the FGCO₂ variability on average ($r = -0.40$) (Table 1). After applying a 5-month lead time to the Nino3.4 index, we find the same El Niño event would explain 26% of the FGCO₂ variability ($r = -0.51$) (Table 5)). Across all systems and the four major climate index predictors, there is really only a strong argument to lead HumCS FGCO₂ anomalies by a few months with ENSO.

CalCS Nino3.4 vs FG_CO2 Cross-Correlations
Nino3.4 Leads to the Left of Zero

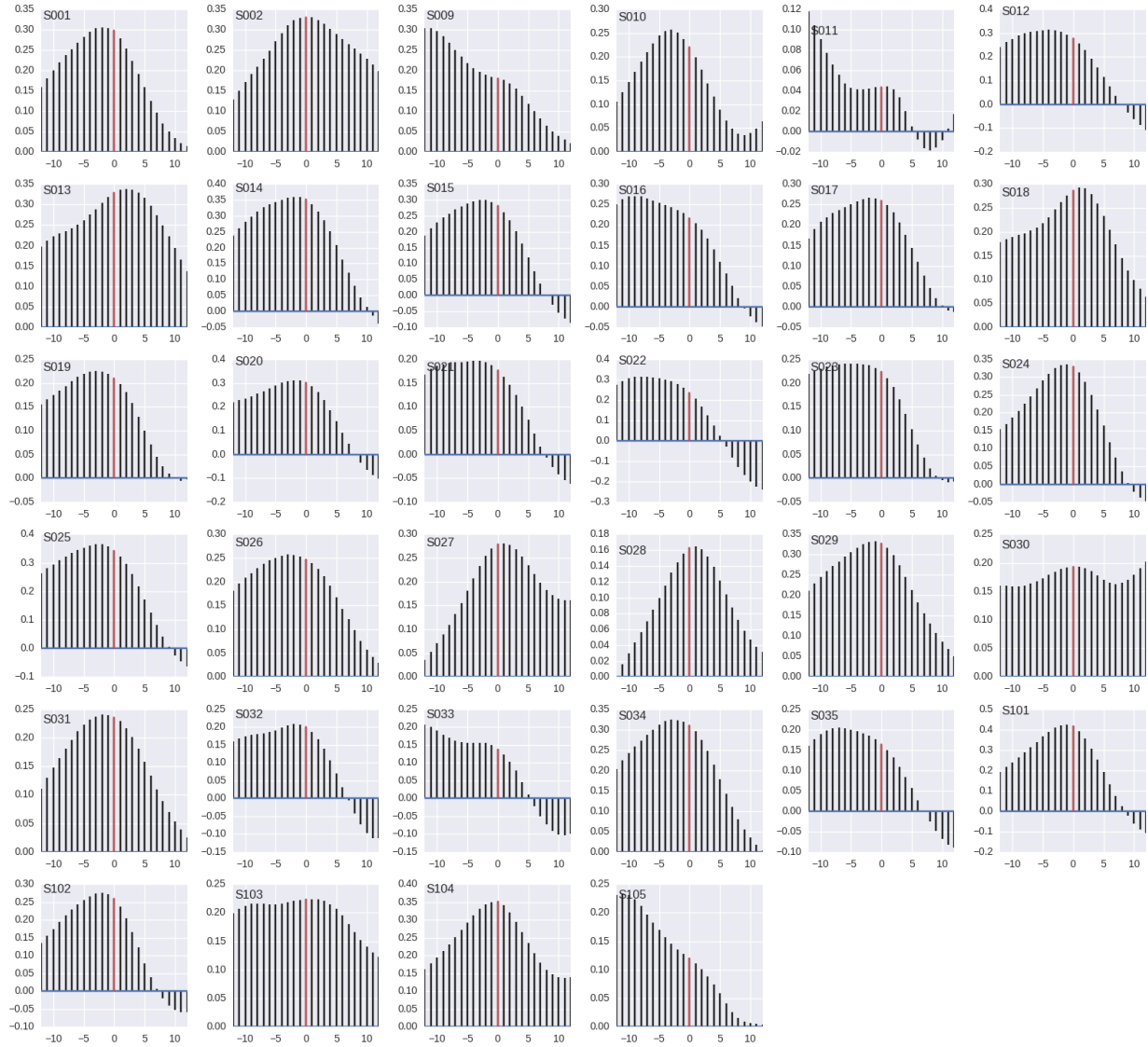


Figure 8: Cross correlations between CalCS FGCO₂ and the Nino3.4 index. Negative values indicate ENSO leading FGCO₂ in months. The red bar indicates no lag for reference.

HumCS Nino3.4 vs FG_CO2 Cross-Correlations
Nino3.4 Leads to the Left of Zero

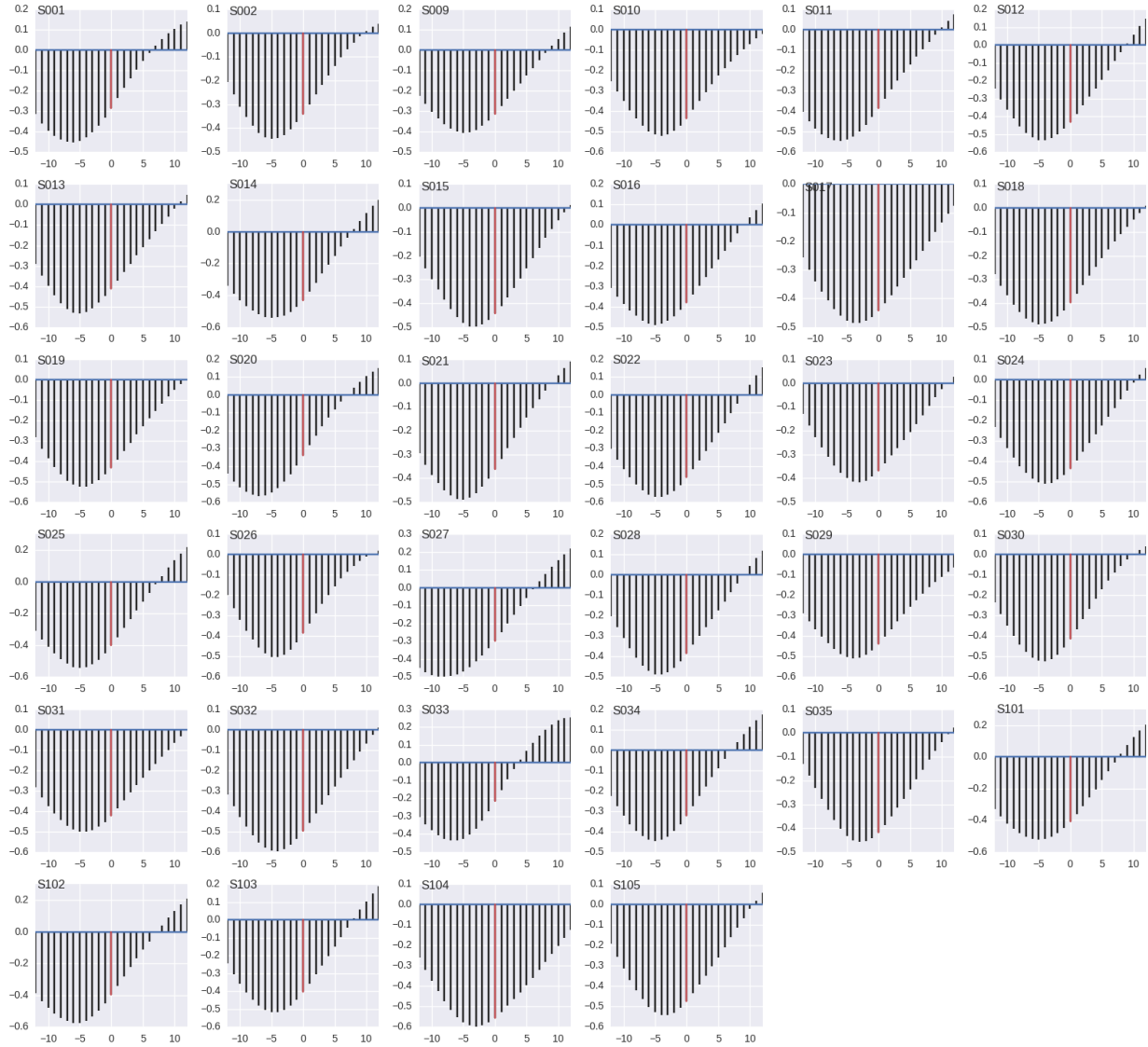


Figure 9: Cross correlations between HumCS FGCO2 and the Nino3.4 index. Negative values indicate ENSO leading FGCO2 in months. The red bar indicates no lag for reference.

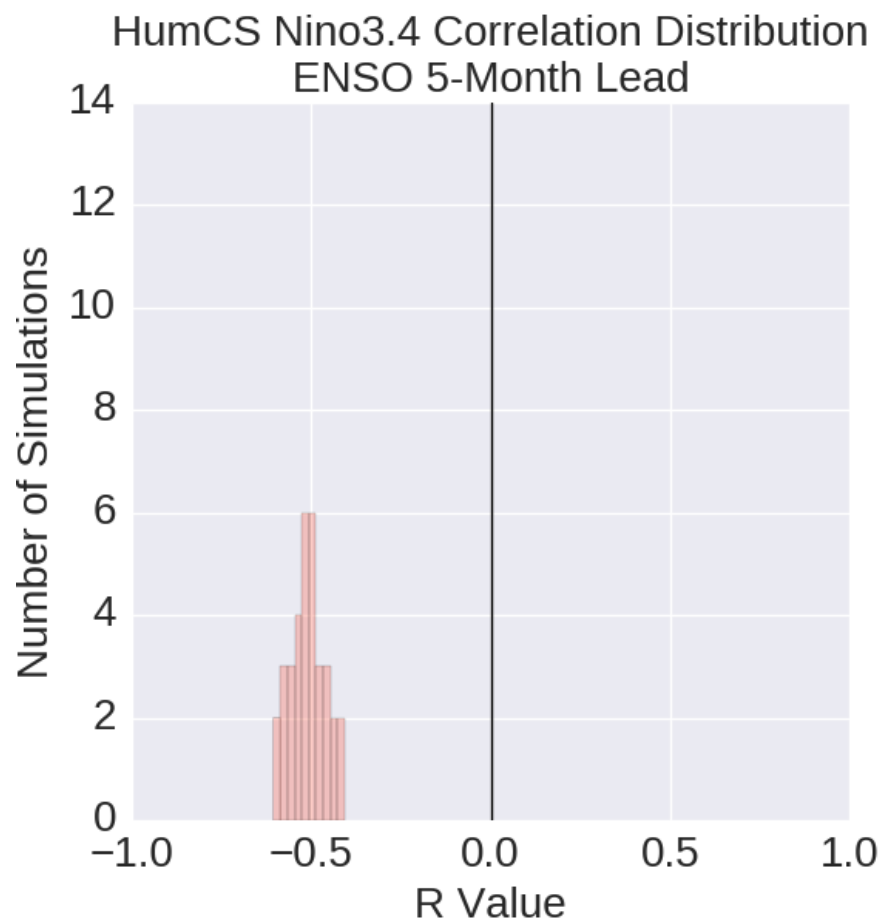


Figure 10: Distribution of r values for a correlation between HumCS FGCO₂ anomalies and the Nino3.4 index with a 5-month lead time.

Table 5: Results for regressing HumCS FGCO₂ anomalies onto Niño3.4 time series with a 5-month lead. Results with $p > 0.05$ are excluded.

Simulation	Slope^a	R	R²
0	-0.31	-0.45	0.20
1	-0.41	-0.46	0.21
2	-0.31	-0.41	0.17
3	-0.40	-0.52	0.27
4	-0.40	-0.55	0.30
5	-0.39	-0.54	0.29
6	-0.43	-0.54	0.29
7	-0.38	-0.56	0.31
8	-0.38	-0.49	0.24
9	-0.41	-0.49	0.24
10	-0.28	-0.48	0.23
11	-0.41	-0.49	0.24
12	-0.43	-0.53	0.28
13	-0.35	-0.58	0.34
14	-0.38	-0.49	0.24
15	-0.45	-0.57	0.33
16	-0.34	-0.41	0.17
17	-0.38	-0.51	0.26
18	-0.40	-0.55	0.30
19	-0.41	-0.50	0.25
20	-0.35	-0.47	0.22
21	-0.33	-0.49	0.24
22	-0.45	-0.52	0.27
23	-0.37	-0.52	0.27
24	-0.41	-0.50	0.25
25	-0.46	-0.61	0.37
26	-0.29	-0.43	0.19
27	-0.34	-0.45	0.20
28	-0.32	-0.43	0.19
29	-0.36	-0.53	0.28
30	-0.35	-0.58	0.34
31	-0.37	-0.52	0.27
32	-0.44	-0.59	0.34
33	-0.50	-0.55	0.30
Mean	-0.38	-0.51	0.26
Std	0.05	0.05	0.05

^a mol/m²/yr/degC

6 Spatial Correlation

The above correlation results are built upon quite large EBUS regions—we generate area-weighted time series over a 1000km meridional and 800km zonal region. What if there are nuances on a finer spatial scale? Perhaps there is some sort of spatial structure, such as an r-value dipole, that we are missing out on.

For the CalCS, FGCO₂ correlations with ENSO are rather homogeneous (Figure 11). In most simulations, we find a consistent positive correlation throughout the study area—during an El Niño, there is an anomalous CO₂ outgassing. However, an interesting structure emerges from correlations with PDO (Figure 12)—the stronger predictor of the two climate indices (Table 2). In a majority of simulations, we find a positive relationship with offshore FGCO₂ and PDO (a positive PDO event causes anomalous outgassing), but a negative relationship with coastal FGCO₂ along California.

For the HumCS, I assess the spatial correlation of FGCO₂, lead by 5 months by ENSO, due to its stronger relationship (see above sections). In general, we find strong negative correlations throughout the offshore region and coastal south-central Peru (Figure 13). In some simulations, we find a similar equatorward dipole as between CalCS FGCO₂ and PDO. Except, in this case, it is of opposing sign. The spatial correlations between HumCS FGCO₂ and PDO shows a clearer emergence of this dipole (Figure 14), although the correlations are weaker overall than with ENSO (a point found in Table 2). An interesting case is the HumCS-AMO relationship. In a number of simulations, the HumCS exhibits an nearshore-offshore dipole between a nearshore positive correlation and offshore negative correlations (Figure 15).

A similar AMO spatial correlation was found for the CanCS, that might induce the weaker negative scores overall (Figure 16).

The spatial correlations between CanCS and ENSO resulted in a pretty consistent positive correlation throughout the region, with no meaningful pattern emergence. Plots were not produced for the BenCS, due to its low or insignificant correlation scores with all of the major climate indices.

CalCS Grid Cell Correlations with ENSO (1920-2015)

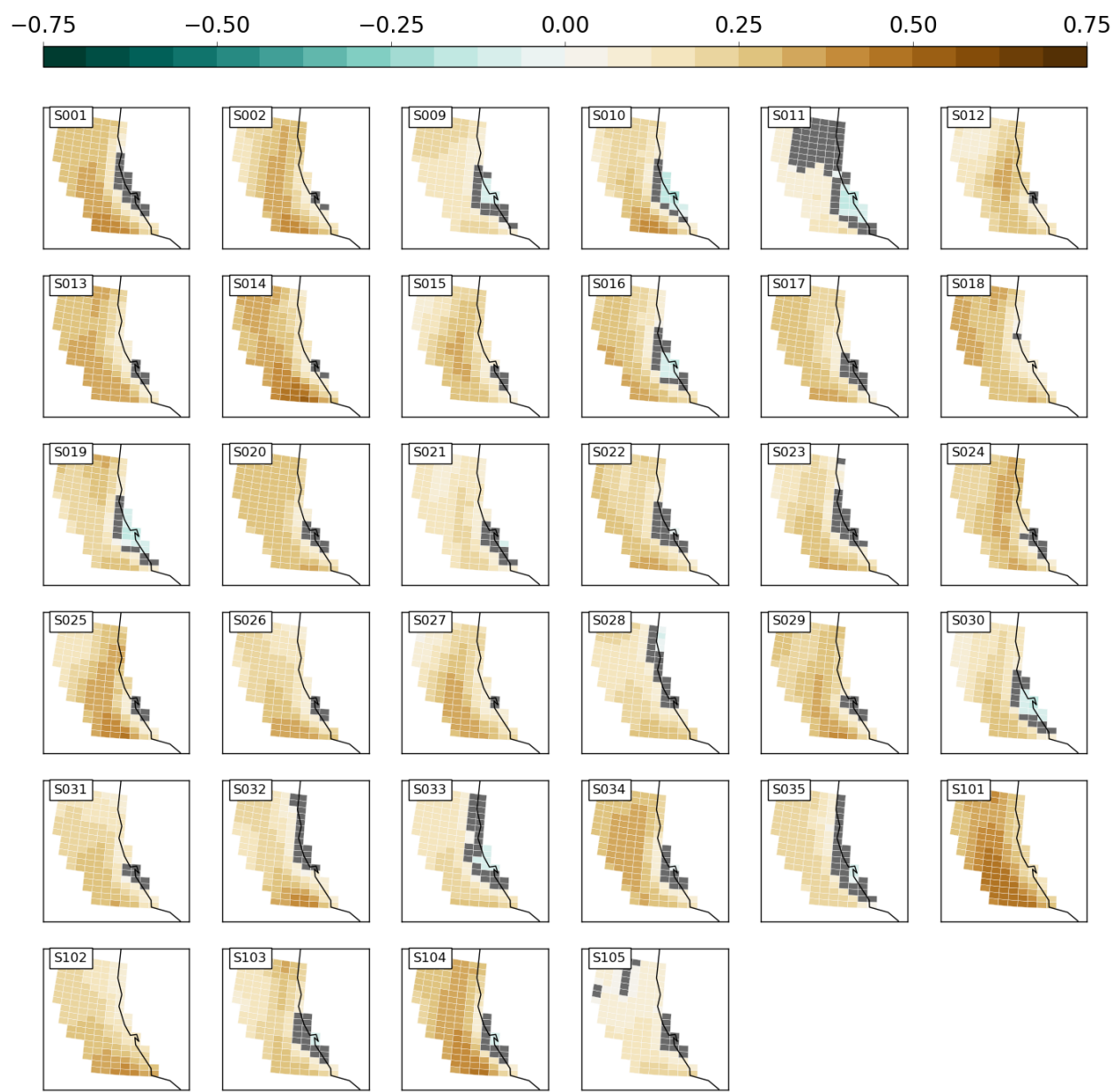


Figure 11: Grid cell correlations with the Niño3.4 index in the CalCS. Brown colors are positive r -values, while blue colors are negative r -values. Gray grid cells were analyzed, but have $p > 0.05$.

CalCS Grid Cell Correlations with PDO (1920-2015)

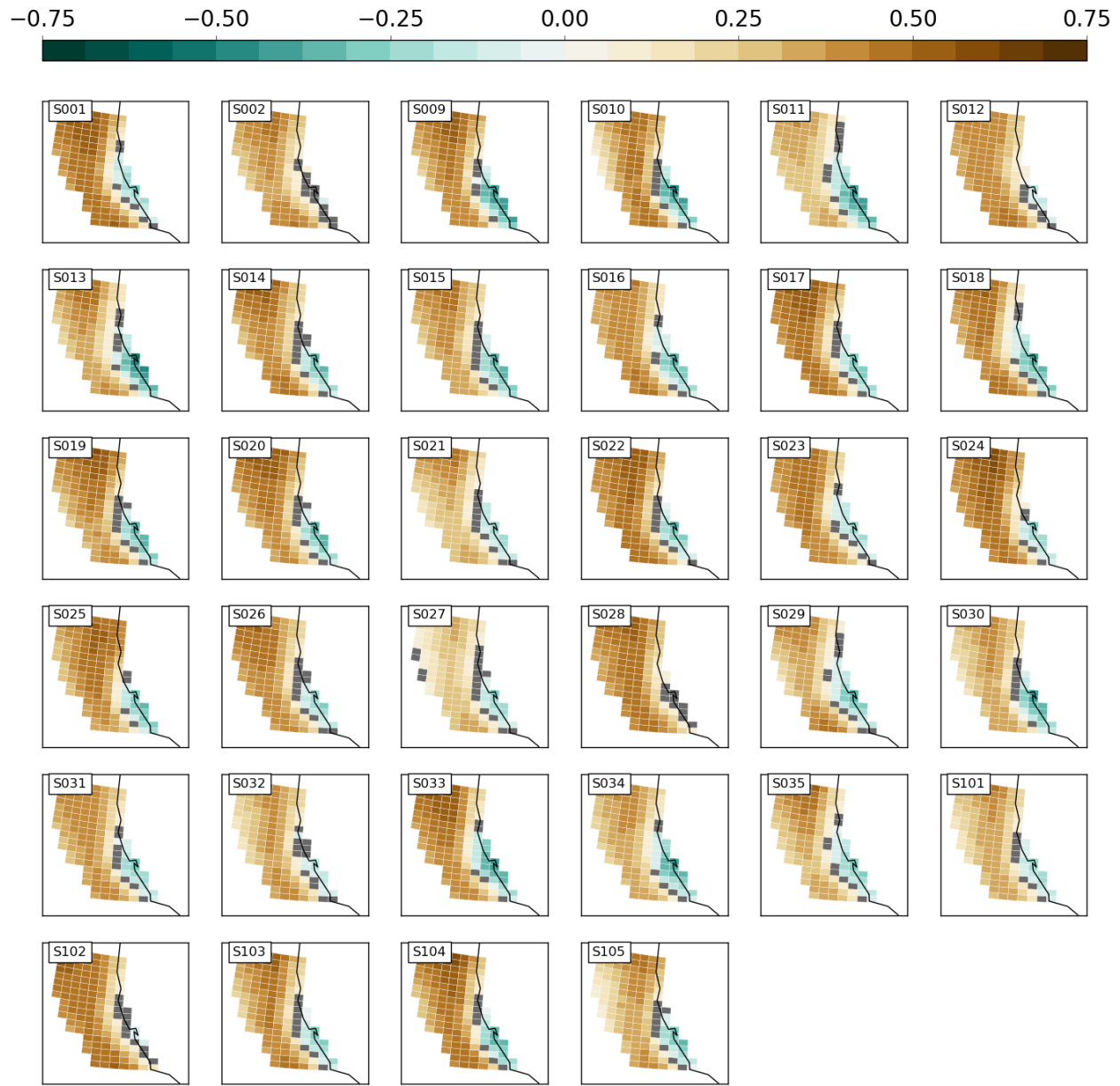


Figure 12: Grid cell correlations with PDO index in the CalCS. Brown colors are positive r -values, while blue colors are negative r -values. Gray grid cells were analyzed, but have $p > 0.05$.

HumCS Grid Cell Correlations with ENSO (1920-2015) ENSO Lead 5

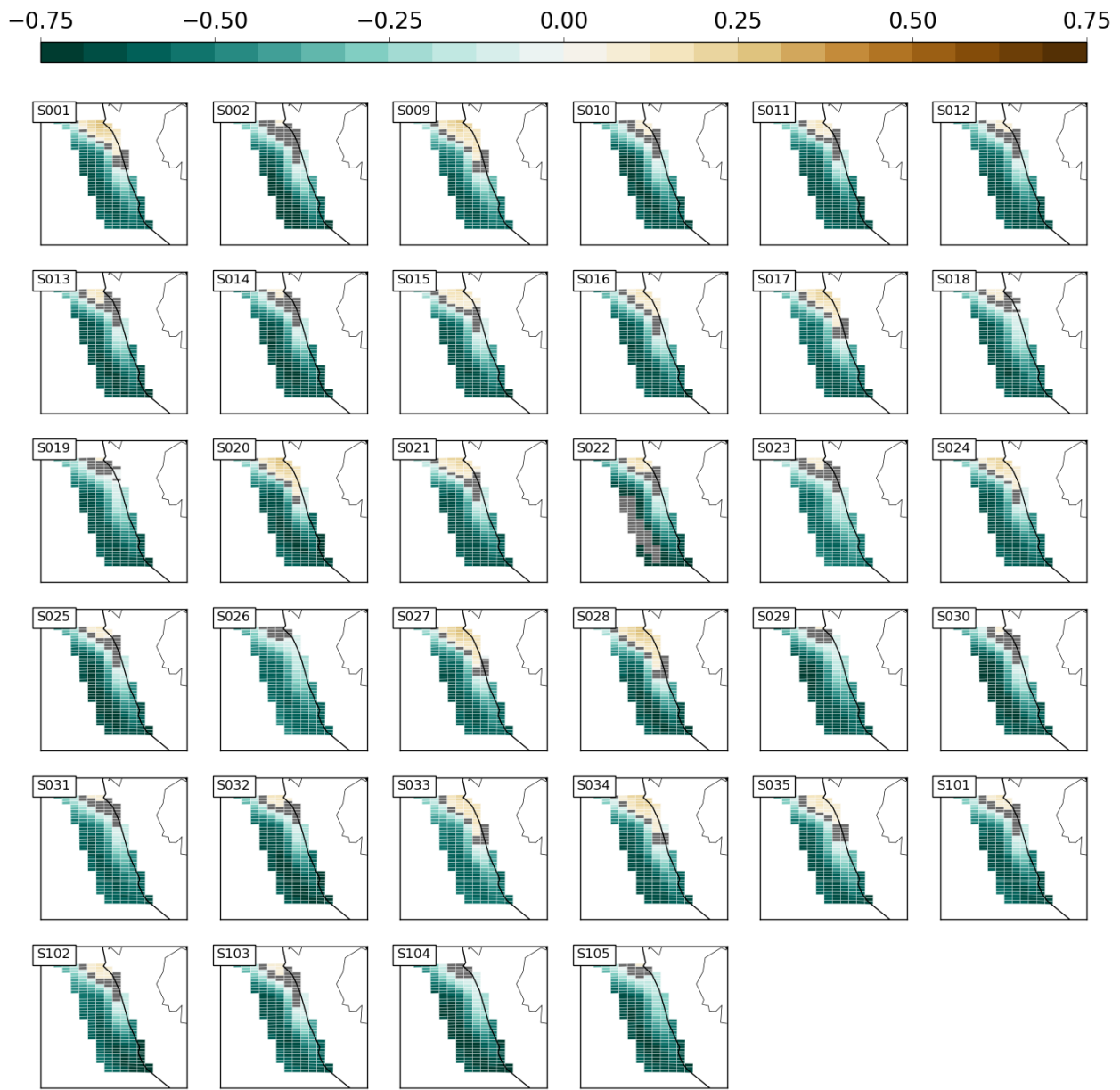


Figure 13: Grid cell correlations with Nino3.4 index (5 month lead) in the HumCS. Brown colors are positive r -values, while blue colors are negative r -values. Gray grid cells were analyzed, but have $p > 0.05$.

HumCS Grid Cell Correlations with PDO (1920-2015)

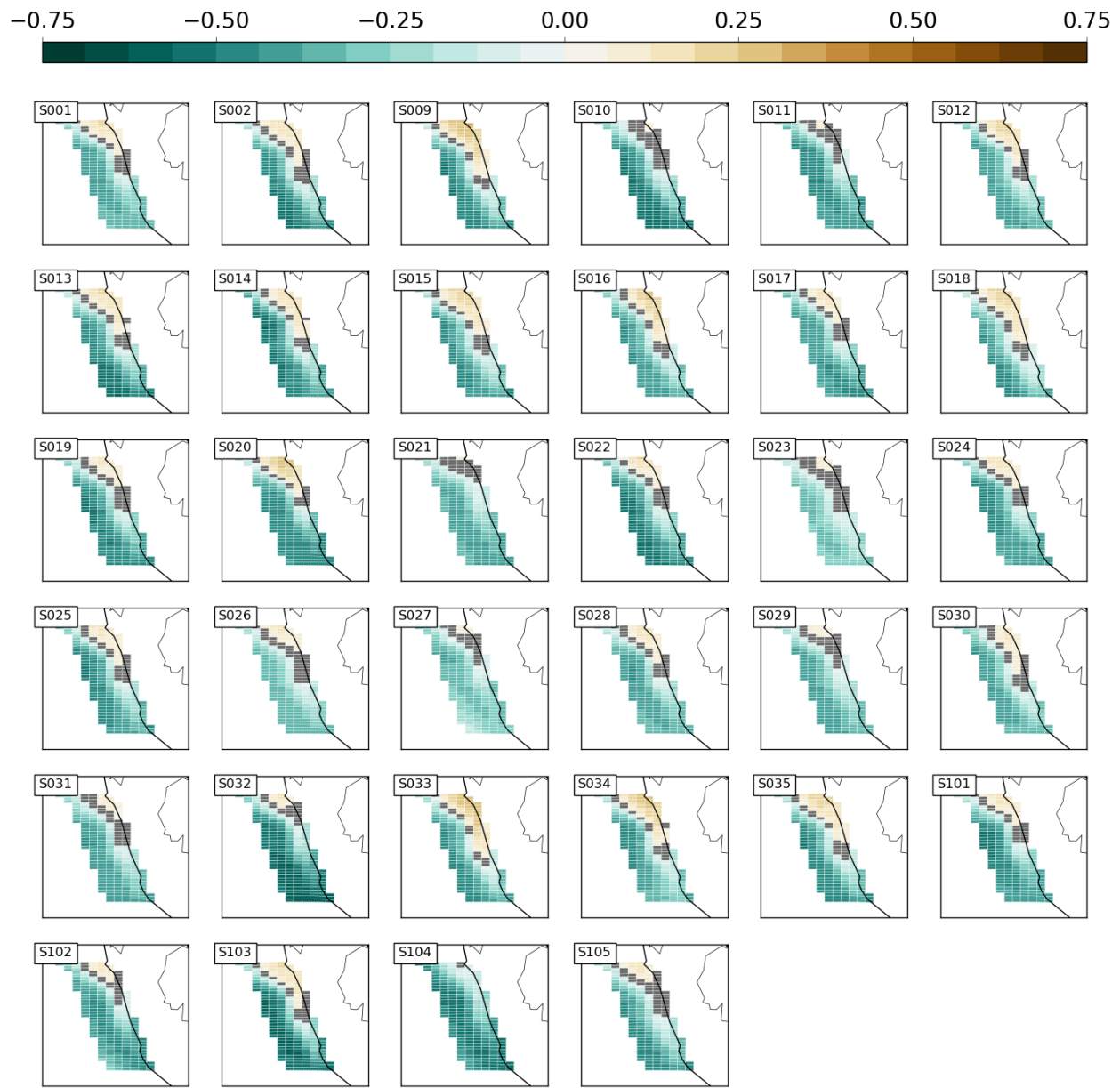


Figure 14: Grid cell correlations with the PDO index in the HumCS. Brown colors are positive r -values, while blue colors are negative r -values. Gray grid cells were analyzed, but have $p > 0.05$.

HumCS Grid Cell Correlations with AMO (1920-2015)

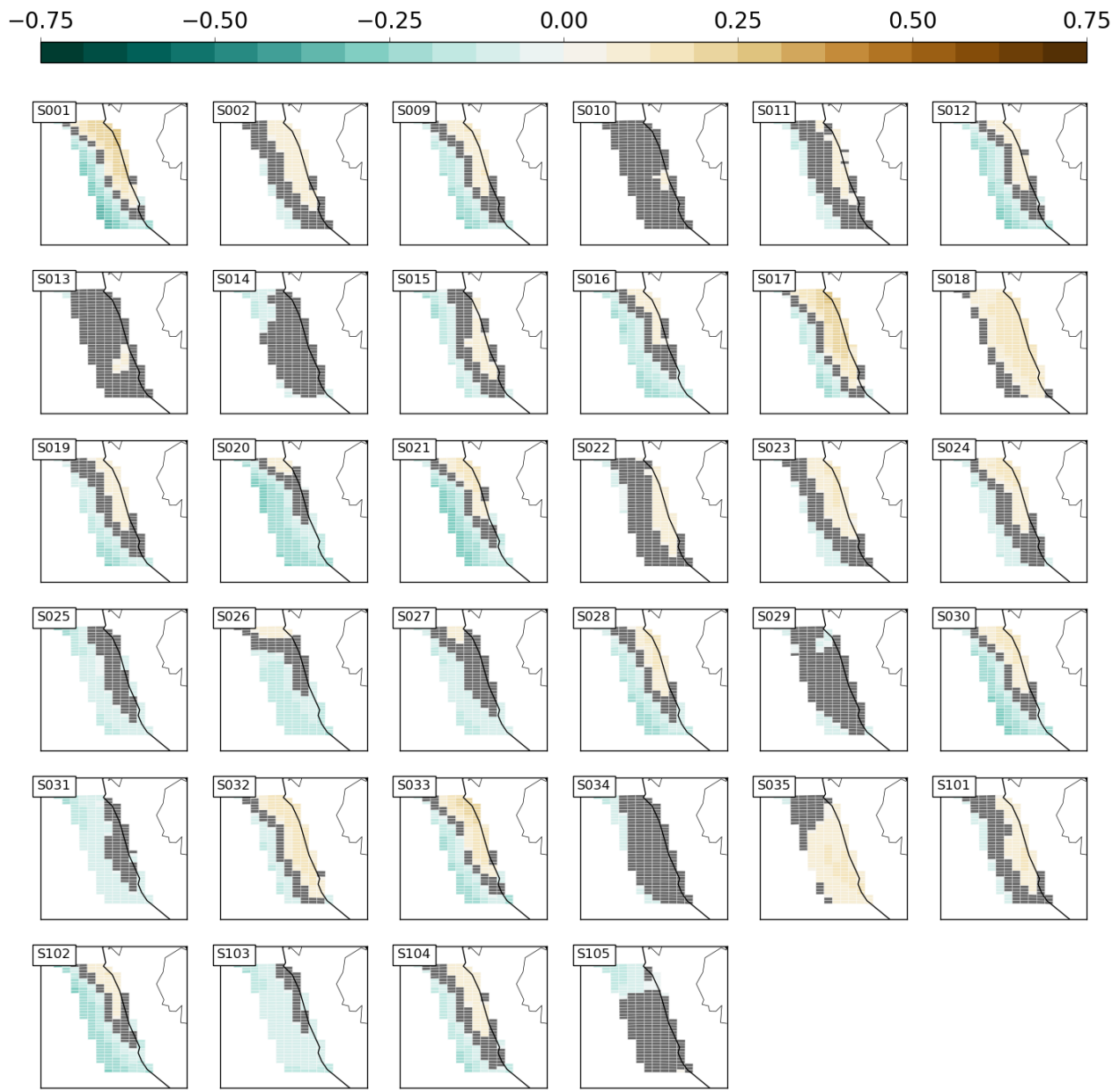


Figure 15: Grid cell correlations with the AMO index in the HumCS. Brown colors are positive r -values, while blue colors are negative r -values. Gray grid cells were analyzed, but have $p > 0.05$.

HumCS Grid Cell Correlations with AMO (1920-2015)

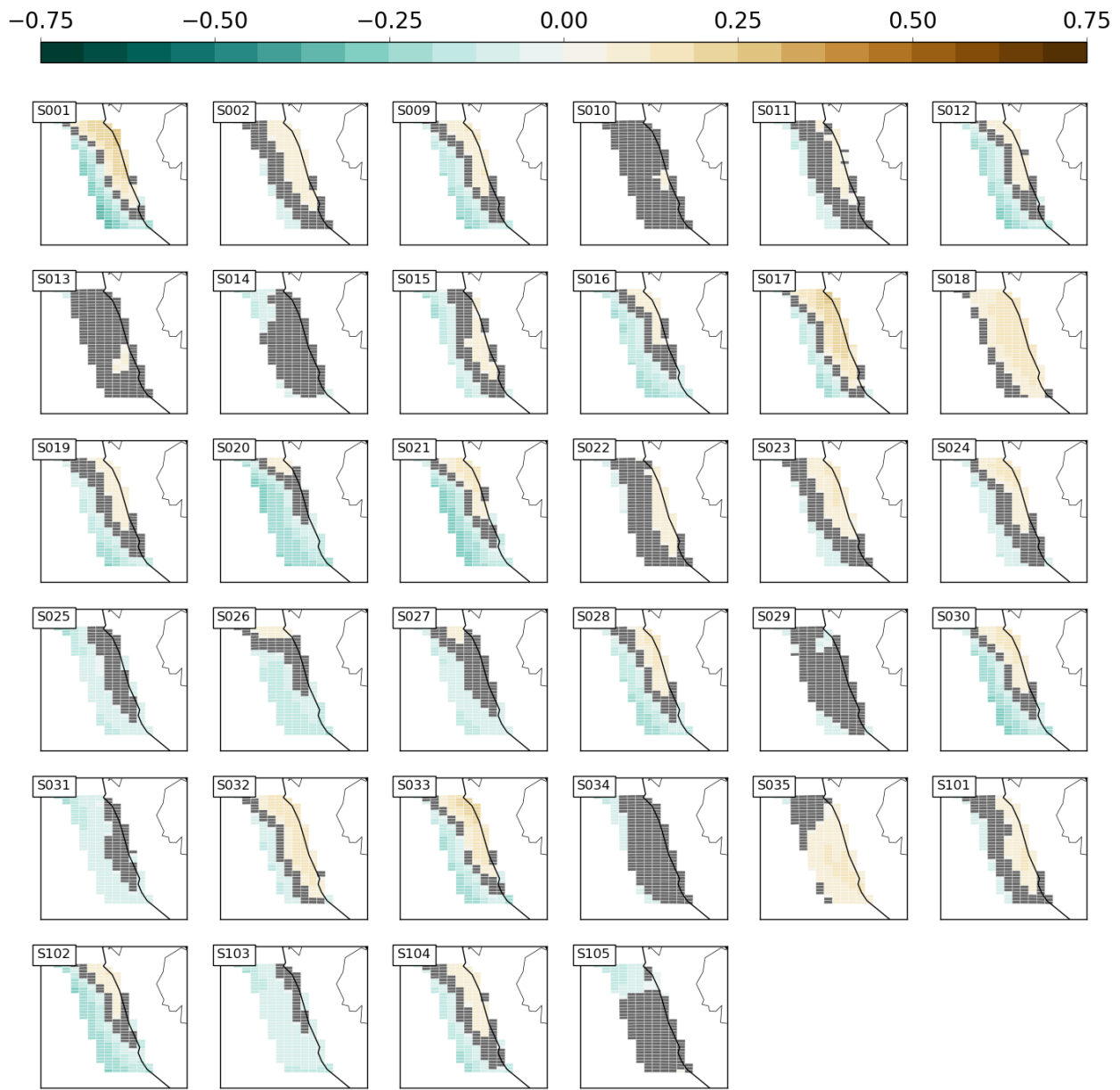


Figure 16: Grid cell correlations with the AMO index in the CamCS. Brown colors are positive r -values, while blue colors are negative r -values. Gray grid cells were analyzed, but have $p > 0.05$.

7 pCO₂/SST Effects

The sea-air CO₂ flux is driven mainly by $\Delta p\text{CO}_2$, the difference between surface ocean and atmospheric CO₂. Since atmospheric CO₂ is relatively stable, we should expect high correlations between ocean pCO₂ variability and FGCO₂. I ran correlations between annual smoothed pCO₂ and annual smoothed FGCO₂ for all four systems, and we find the expected positive relationship for *every* simulation across *every* system. R values are generally greater than 0.95 (Figure 17). High pCO₂ anomalies lead to outgassing.

So, there isn't much to be learned from that exercise. More importantly, what is the major control on pCO₂ variability in each system? A good starting point is SST, which controls the solubility of CO₂. Figure 18 displays the results of correlations between SST anomalies and FGCO₂ anomalies in all four EBUS. The CalCS behaves as one might expect a solubility-dependent system to act. When there are warm SST anomalies, there is anomalous outgassing in the system (Figure 19). On the other hand, the HumCS is well-explained by SSTs in an opposing fashion. Warm SST anomalies actually lead to an anomalous uptake of CO₂ (Figure 20). This is certainly not a direct causation, but rather the warm SST anomalies are linked to some other process. I would assume in this case, warm SST anomalies are linked to processes such as ENSO that would deepen the thermocline, leading to CO₂- (and nutrient-) deprived waters being upwelled. Perhaps the HumCS is more controlled by DIC concentrations than by solubility.

The CanCS exhibits similar features to the HumCS in terms of SSTs, but to a fairly weak degree (Figure 21). And as we have become so used to, the BenCS is not really explained by SST variability at all (Figure 22).

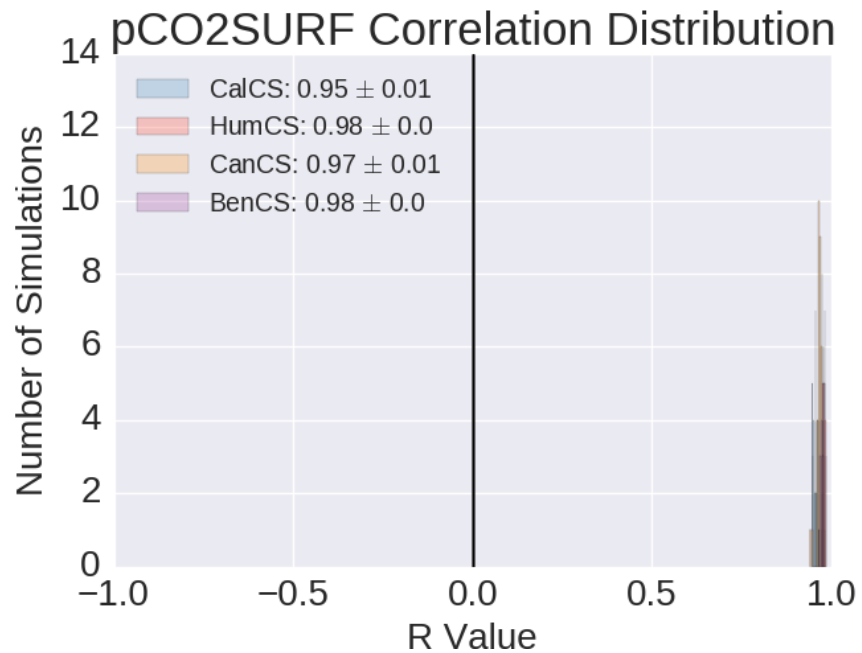


Figure 17: Correlation results between $p\text{CO}_2$ and FGCO_2 across all systems. Simulations with $p > 0.05$ were excluded.

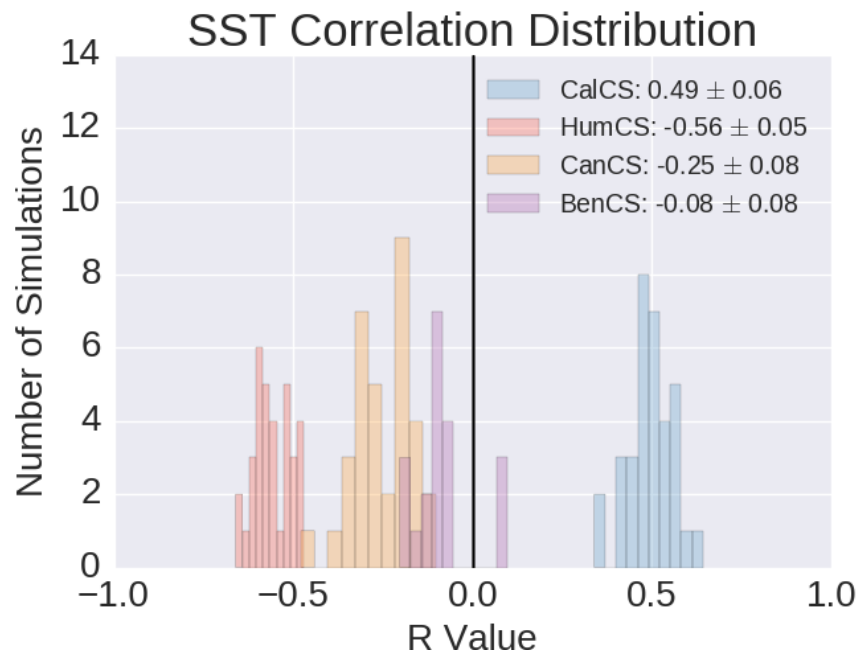


Figure 18: Correlation results between SST and FGCO_2 across all systems. Simulations with $p > 0.05$ were excluded.

CalCS SST-FG_CO2 Anomaly Regression (1920-2015)

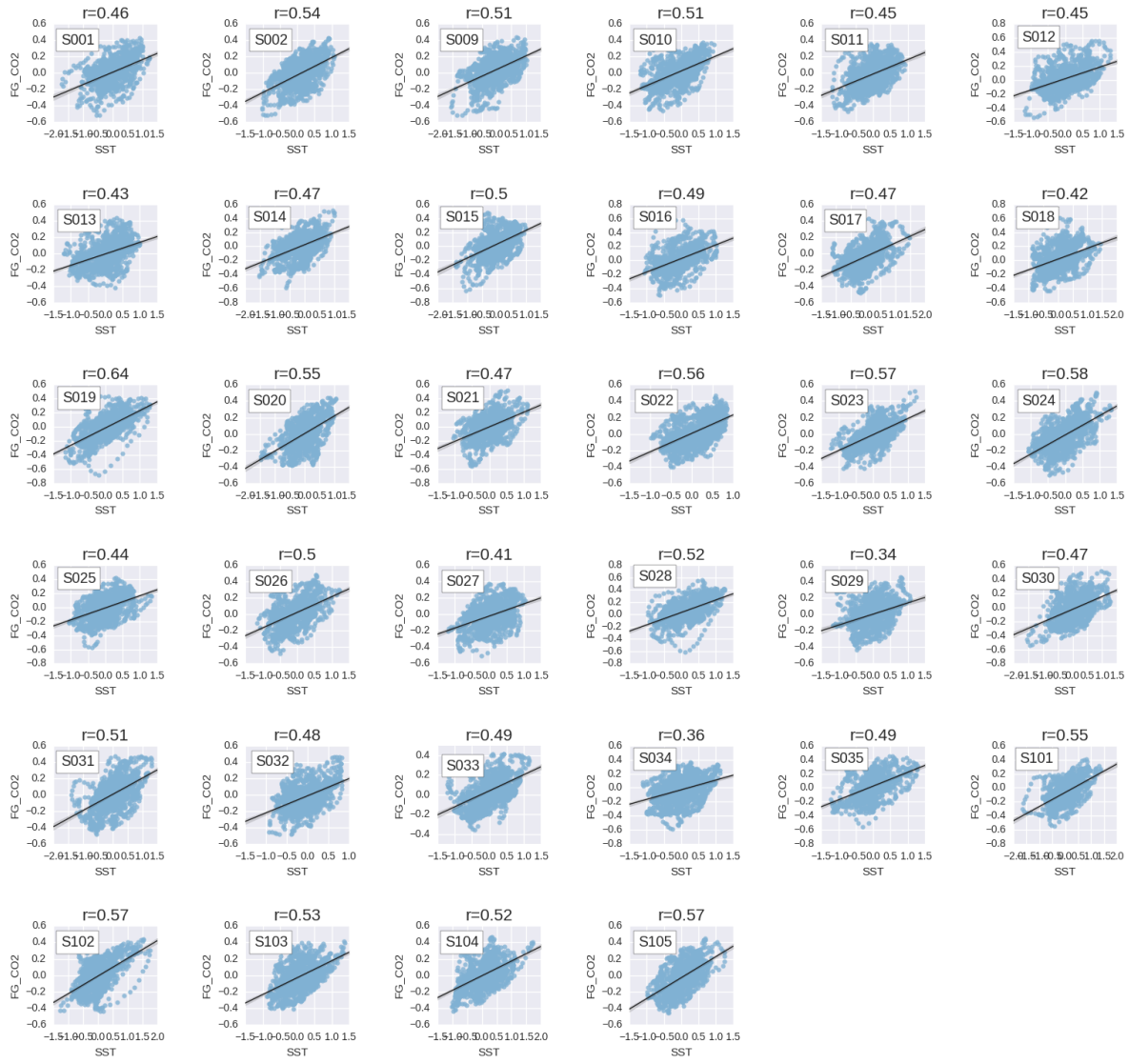


Figure 19: Regression analysis between SST and FGCO2 in the CalCS.

HumCS SST-FG_CO2 Anomaly Regression (1920-2015)

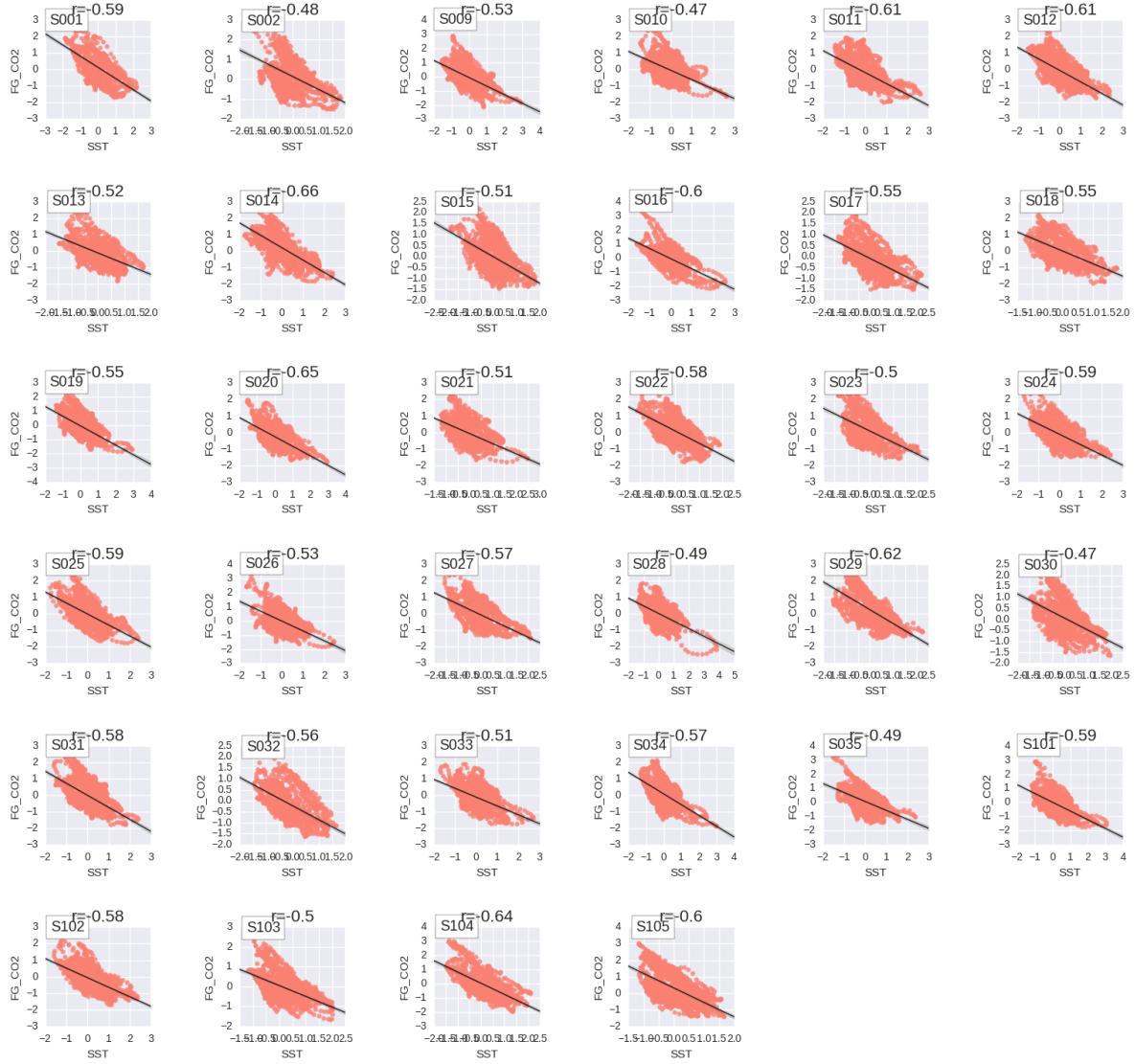


Figure 20: Regression analysis between SST and FGCO₂ in the HumCS.

CanCS SST-FG_CO2 Anomaly Regression (1920-2015)

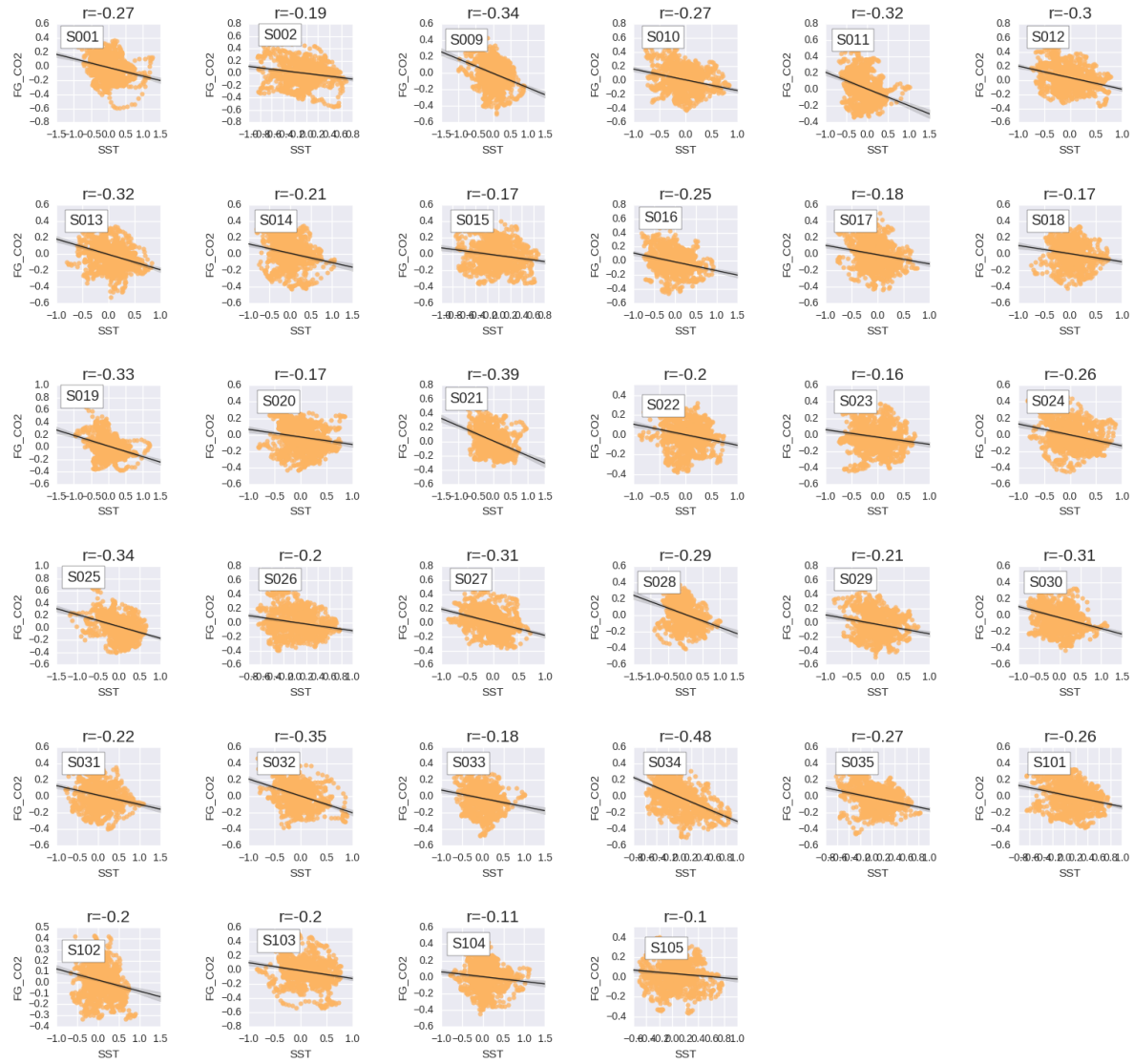


Figure 21: Regression analysis between SST and FGCO2 in the CanCS.

BenCS SST-FG_CO2 Anomaly Regression (1920-2015)



Figure 22: Regression analysis between SST and FGCO2 in the BenCS.

References

- Francisco P. Chavez and Monique Messié. A comparison of Eastern Boundary Upwelling Ecosystems. *Prog. Oceanogr.*, 83(1-4):80–96, 2009. ISSN 00796611. doi: 10.1016/j.pocean.2009.07.032. URL <http://dx.doi.org/10.1016/j.pocean.2009.07.032>.
- P. Landschützer, N. Gruber, D. C E Bakker, U. Schuster, S. Nakaoka, M. R. Payne, T. P. Sasse, and J. Zeng. A neural network-based estimate of the seasonal to inter-annual variability of the Atlantic Ocean carbon sink. *Biogeosciences*, 10(11):7793–7815, 2013. ISSN 17264170. doi: 10.5194/bg-10-7793-2013.
- Goulven G. Laruelle, Peter Landschützer, Nicolas Gruber, Jean-Louis Tison, Bruno Delille, and Pierre Regnier. Global high resolution monthly pCO₂ climatology for the coastal ocean derived from neural network interpolation. *Biogeosciences Discuss.*, (February):1–40, 2017. ISSN 1810-6285. doi: 10.5194/bg-2017-64. URL <http://www.biogeosciences-discuss.net/bg-2017-64/>.
- Taro Takahashi, Stewart C Sutherland, Colm Sweeney, Alain Poisson, Nicolas Metzl, Bronte Tilbrook, Nicolas Bates, Rik Wanninkhof, Richard a Feely, Christopher Sabine, Jon Olafsson, and Yukihiro Nojiri. Global sea air CO₂ flux based on climatological surface ocean pCO₂, and seasonal biological and temperature effects. *Deep Sea Res. Part II Top. Stud. Oceanogr.*, 49(9-10):1601–1622, 2002. ISSN 09670645. doi: 10.1016/S0967-0645(02)00003-6. URL <http://linkinghub.elsevier.com/retrieve/pii/S0967064502000036>.